



Structural design and high temperature tribological behavior of a new turbine blade tip protective coating

Shuai Yang, Siyang Gao^{*}, Weihai Xue, Bi Wu, Deli Duan^{*}

School of Materials Science and Engineering, University of Science and Technology of China, Shenyang 110016, PR China

Institute of Metal Research, Chinese Academy of Sciences, Shi-changxu Innovation Center for Advanced Materials, Shenyang 110016, PR China

ARTICLE INFO

Keywords:

NiAlTa coating
Electro spark deposition
Blade tip coating
Structural design
Wear resistance

ABSTRACT

Severe damage to the blade tip usually occurs when the turbine blade tip scratches against the abrasible coating. Therefore, blade tip strengthening is a hot research topic. To improve the wear resistance of turbine blade tips, NiAlTa coatings were prepared on K417G superalloy by electro spark deposition. The microstructure and phase composition of the coating were analyzed by scanning electron microscope and X-ray diffraction. Microhardness tester and scratch method were used to test the microhardness and bonding strength of the coating. Using ZrO₂ balls as friction pair, the tribological behavior and wear mechanism of the coating were investigated by a self-developed tribometer at 25 °C and 800 °C. The NiAlTa coating mainly consists of the β phase NiAl and the laves phase NiTaAl. The laves phase NiTaAl encapsulates the NiAl phase, and this plant-like “cell wall” structure endows the coating with excellent mechanical properties, wear resistance, and cutting performance. Compared with the substrate, NiAlTa coating has higher microhardness (~797.18 HV_{0.2}) and lower wear rate (~10⁻⁶ mm³·N⁻¹·m⁻¹). The wear process of NiAlTa coatings is dominated by plastic deformation, with little evidence of material loss from the brittle fracture. The competition between the anti-wear lubricating effect of the “glaze” layer and the plowing effect of oxides and ZrO₂ debris affects the tribological behavior of the coating. The cutting performance of the NiAlTa coating can be attributed to the two-body or three-body abrasive wear caused by the oxides and ZrO₂ debris embedded in the “glaze” layer.

1. Introduction

The efficiency of an aeroengine is highly dependent on the clearance between the rotating blades and the stationary case. If the clearance is extremely large, then the compressed air will escape from the top of the blade, reducing the efficiency of the aeroengine [1]. The seal between the blades and the case in the high-pressure turbine is particularly crucial in preventing such losses. The sealing method of cutting the abrasible sealing coating applied to the surface of the case to form a specific track is gradually being used.

The turbine blade tip is difficult to study due to its ultra-high linear velocity (> 400 m/s), the instantaneous ultra-high temperature (>1000 °C) generated during the rub-impact process, and its complex interaction with the environment (such as salt spray, sand, and dust). Designing testers for harsh conditions (e.g., high temperature/high-speed rubbing machine) is also a great challenge. Therefore, few studies have been reported on the design and evaluation of protective coatings for turbine blade tips [2,3]. In addition, as the turbine inlet

temperature and pressure continue to rise, the abrasible sealing coating applied to the casing surface gradually develops into a high-hardness ceramic sealing coating (such as 8 % Y₂O₃ stabilized ZrO₂, YSZ), which exacerbates the occurrence of blade tip wear, oxidation, and cracking [4]. This phenomenon seriously affects the air path sealing performance of aeroengines. Therefore, the design and evaluation of protective coatings for turbine blade tips are urgent and necessary tasks..

In sliding two-body abrasive wear, abrasion of one body is caused by hard protrusions or particles attached to the other body, which are not free to roll. This leads generally to a higher rate of wear than if the particles are permitted to roll, as in three-body abrasion. Therefore, to ensure effective cutting and protect the blade tips from wear, the initial blade tip protective coatings are designed based on the two-body abrasive wear concept. Currently, the reported blade tip protective coatings are mainly composed of a ductile metal matrix and hard ceramic particles, such as NiCoCrAlY/cBN [5], NiCoCrAlY/Al₂O₃ + ZrO₂ [2], and NiCrAlYSi+NiAl/cBN [6] systems prepared by typical composite electrodeposition (Tribomet process), direct laser deposition,

^{*} Corresponding authors at: School of Materials Science and Engineering, University of Science and Technology of China, Shenyang 110016, PR China.

E-mail addresses: sygao@imr.ac.cn (S. Gao), dlduan@imr.ac.cn (D. Duan).

<https://doi.org/10.1016/j.surfcoat.2023.129316>

Received 23 October 2022; Received in revised form 23 January 2023; Accepted 3 February 2023

Available online 9 February 2023

0257-8972/© 2023 Elsevier B.V. All rights reserved.

low-pressure plasma spraying, aluminizing, and other techniques. However, the NiCoCrAlY system can no longer meet the current operating environment of high-temperature turbines because of problems such as the low high-temperature strength of the metal matrix (the creep rate of MCrAlY increases exponentially with the temperature, which is conducive to melt wear) and severe adhesive wear [2,7]. Furthermore, the selection of hard ceramic particles and their bonding with the metal matrix are particularly prominent issues. During service, the hard ceramic particles embedded in the metal matrix often fail by dislodging, oxidizing, or even fracturing and cannot achieve repeated cutting and wear prevention throughout the life cycle of turbine engines [2,8]. In addition, the preparation techniques of blade tip protective coatings have been gradually developed and applied and progressively evolved in the direction of improving the bonding strength of coatings and avoiding blade damage.

On this basis, we abandon the concept of two-body abrasive wear and propose a “coating + preparation technology” blade tip protective coating system. The new coating is a laves phase NiTaAl reinforced NiAl coating. The NiAl coating, as the first generation of blade protection coating, has excellent environmental resistance (such as oxidation resistance and wear resistance). Meanwhile, the modulus of elasticity and coefficient of thermal expansion of NiAl are similar to those of nickel-based superalloys. Therefore, NiAl does not cause excessive thermal stress when assembled with nickel-based superalloys [9]. However, single NiAl coating is insufficient to bear 1200 °C, and the limited slip system, the large slip vector, and the restricted cross-slip make the effective coordination of the local deformation in the low-temperature deformation and exhibition of high low-temperature brittleness difficult for the NiAl phase [10]. The above problems can be solved by the technical means commonly used by researchers, such as alloying and grain refinement. The laves phase NiTaAl has been shown to have excellent high temperature and wear resistance [11], so the selected alloying element is the high melting point Ta element. Rapid solidification techniques (e.g., laser cladding and electro spark deposition) can be used to obtain coatings with metallurgical bonding strength and significant grain refinement and simultaneously improve the strength and toughness of alloys. However, considering the unique characteristics of the blade tip (such as high crack sensitivity and thin-walled structure), the laser cladding technique with a high heat input is abandoned. Therefore, the electro spark deposition technique is adopted as the preparation technology.

Electro spark deposition (ESD) is a surface modification technique that uses the spark discharge principle. In protective gases or special fluids (such as argon, kerosene), the workpiece is used as the negative electrode and the rod-shaped conductive material as the positive electrode. The high energy electrical energy stored by the power supply causes a high frequency pulse spark discharge or arc discharge between the conductive material and the metal workpiece. In a very short time of 10^{-6} – 10^{-5} s, a current density of 10^5 – 10^6 A/cm² can be generated at the tiny part of the contact, producing an instantaneous high temperature of 8000–25,000 K. The high-density energy makes the workpiece and the electrode material melt at the same time, and the molten material is transferred to the surface of the workpiece under the joint action of electric field force, centrifugal force, and contact force, etc. ESD has an ultra-high temperature gradient (10^7 – 10^9 K/m), an ultra-fast cooling rate (10^5 – 10^6 K/s), and a low heat input, which is suitable for thin-walled structures (such as the blade tip) [12]. Laser processing is one of the most popular surface modification techniques, but the large heat-affected zone (> 100 μm) makes surface modification of thin-walled parts difficult. Besides, the microfissure is more likely to occur due to the complexity of processing control, it will put highly stressed airfoil in risk [12]. Therefore, the laser processing is not suitable for blade tips. ESD has the unique technical advantages of simple equipment, easy operation, small substrate deformation, and high coating bonding strength, making it an important technical tool in the field of surface engineering and remanufacturing engineering.

In this work, a preliminary evaluation of the proposed “coating and its preparation technology” system was conducted. The coating obtained by this novel system consists of the nano sized phase NiAl and the continuously distributed mesh laves reinforced phase NiTaAl. The high-temperature tribological performance of the coating under the operating environment of the turbine blade tip was studied and evaluated. The laves phase NiTaAl encapsulates the NiAl phase, and this plant-like “cell wall” structure endows the coating with excellent mechanical properties, wear resistance, and cutting performance. In this paper, the concept of two-body abrasive wear is abandoned. The rough surface of the ESD coating is used as the cutting unit instead of hard ceramic particles to effectively cut the ceramic-base sealing coating.

2. Material and methods

2.1. Preparation of coatings

The base material was K417G nickel-based superalloy (Institute of Metal Research, Chinese Academy of Sciences, CHINA), and its chemical composition was listed in Table 1. Several samples were removed from the K417G alloy using wire-cut electrical discharge machining (WEDM). The samples were successively ground with 400#, 800#, 1000#, and 1200# SiC sandpapers. An Al₂O₃ polishing paste with a particle size of 2.5 μm was used for polishing to a specified roughness (Ra ≈ 0.6 μm, and this roughness value is near those of real bare blades.). Finally, the samples were placed in ethanol for ultrasonic cleaning for 20 min and blow-dried ready for use.

NiAlTa coatings were prepared as follows:

- (1) Ingredients: Ni, Al, and Ta metal raw materials (Hefei City Shushan District Weng Hou Metal Materials Trading Company, CHINA) with a nominal purity of 99.999 % were selected. After being polished off the surface oxide, the Ni, Al, and Ta raw materials were weighed according to a certain mass ratio (as shown in Table 1). The target mass of the alloy ingot is 70 g. Given that the boiling point of Al (2467 °C) is lower than the melting point of Ta (2996 °C), the Al raw material must be compensated. In this paper, the actual mass of Al is 1.05 times the theoretical mass.
- (2) Preparation of NiAlTa alloy ingots by arc melting: The weighed raw materials were placed in a non-consumable arc melting furnace (Institute of Metal Research, Chinese Academy of Sciences, CHINA) in order of melting point from low to high. After vacuuming the furnace body (2.5×10^{-3} Pa), the furnace was filled with inert gas (Ar) to 0.05 Pa. Smelting was carried out under the protection of inert gas. In this case, the melting current was 232 A, and the melting time was 60 s. After cooling the samples, they were turned over using crucible tongs and continued to be melted, and the NiAlTa alloy ingots were obtained by repeated melting six times.
- (3) Preparation of bar electrodes by wire cutting: Several bar electrodes with a diameter of 4 mm and a length of 30 mm were removed from the alloy ingot by WEDM. One end of the electrode rods was ground into a hemisphere, and they were ground and polished. They were ultrasonically cleaned in ethanol for 20 min and blow-dried for later use.
- (4) Preparation of coatings using electro spark deposition: The pre-treated K417G substrate was connected to the negative electrode and the electrode rod was connected to the positive electrode. The NiAlTa coatings were prepared by 3H-ES6 type electro spark deposition equipment (Institute of Metal Research, Chinese Academy of Sciences, CHINA), and the specific preparation parameters were shown in Table 2. Fig. 1a showed a schematic diagram of the electro spark deposition principle. The thickness of the coatings was maintained at 50–70 μm.

Table 1
Chemical composition of K417G substrate and NiAlTa coating (wt%).

	Ni	Co	Cr	Al	Mo	Ti	C	B	Zr	V	Ta
K417G substrate	Bal.	10.0	9.0	5.25	3.0	4.4	0.17	0.018	0.07	0.75	–
NiAlTa coating	46.85	–	–	21.25	–	–	–	–	–	–	31.89

Table 2
Parameters of electro spark deposition.

Parameters	Value
Working voltage(V)	65
Pulse frequency(Hz)	305
The output power(W)	1500
Electrode rotation speed(r/min)	1300
Guard gas flow(L/min)	15
Tilt angle(°)	60

2.2. Adhesion strength test

The adhesion strength between the coating and the substrate was one of the important indicators of the comprehensive performance of the coating. The adhesion strength was measured by the scratch method. Scratch tests were performed according to ASTM C1624–05 standard. MTF-5000 multi-functional friction and wear tester equipped with HRC-3 Rockwell indenter (RTEC, USA) was used. The test parameters were as follows: loading speed 50 N/min, maximum load 100 N, scratching speed 2 mm/min and scratching length 4 mm. The loading mode was continuous and linear loading. The parameters such as friction force and acoustic signal were recorded during the experiment. After the experiment, the scratch morphology was observed by an optical microscope, and the critical loads of the main failure events during the scratching process were obtained. The critical load was the average value of three scratch tests.

2.3. Wear test

The tribotests were conducted on a self-developed high-temperature tribometer (Institute of Metal Research, Chinese Academy of Sciences, CHINA) with a rotation mode of ball-on-disc configuration. The experimental principle was shown in Fig. 1b. The lower specimen discs were K417G substrate and NiAlTa coating ($\Phi 40$ mm \times 5 mm). ZrO₂ balls (Grade G5, Institute of Metal Research, Chinese Academy of Sciences, CHINA) of 4 mm diameter (1215 HV_{0.5}) were used as the upper sample. ZrO₂ balls were selected as a counterpart sample because of the following reasons. One, ZrO₂ is used as a gas path sealing material in aeroengines. Therefore, NiAlTa coating interacts with ZrO₂ in practical applications. ZrO₂ balls were also used to guide the structural design of the blade tip protective coating by observing the wear behavior of the NiAlTa coating with ZrO₂. A new friction pair was used in the tribotest at each temperature.

The tribotests were carried out at 25 °C and 800 °C. When the corresponding test temperature was reached, it was maintained for 5 min to

ensure that both upper/lower specimens reach a stable temperature. The test parameters were listed in Table 3. The experimental parameters selected are based on extensive literature research to make the experiments comparable and repeatable. During the test, the shear force (F_x) and normal load (F_z) were monitored in real-time, and F_x/F_z was used as the friction coefficient. Other relevant data were also collected and analyzed. Each test was repeated three times to ensure the reproducibility of the results. Microhardness and wear tests were carried out as per ASTM E384 and G99 standards.

2.4. Material characterization

A TESCAN MIRA3 field emission scanning electron microscope (TESCAN, CZECH), a VHX-6000 ultra-depth three-dimensional microscope (KEENSCH, JAPAN), and an Ultim MaxN silicon drift energy spectrometer (OXFORD, UK) were used to analyze the original surface, worn surface, and elemental composition of the substrate and the coating. A D/Max-2500PC X-ray diffractometer (RIKEN, JAPAN) was used to determine the phase composition of both the deposited coatings and the oxidation products of the coatings (Cu K α , 5°/min, 20°–90°). The chemical composition of the worn and unworn surfaces was characterized by Raman spectroscopy (Labram HR Evolution Instrument, HORIBA, JAPAN). The laser wavelength was 532 nm.

A 2300A-R contact profiler (Harbin Gauge & Cutting Tools Group Co., LTD., CHINA) and an ultra-depth three-dimensional microscope were used to analyze the 2D profiles and worn surfaces of the K417G substrate, the NiAlTa coating, and the ZrO₂ balls. According to Eqs. (1) and (2), the wear volumes of the K417G substrate, the NiAlTa coating, and the ZrO₂ balls were calculated as follows:

$$V = 2\pi Sr \quad (1)$$

where V is the wear volume of the NiAlTa coating, mm³; S is the average cross-sectional area of the wear track, mm²; and r is the radius of the

Table 3
High-temperature friction and wear tests parameters.

Parameters	Value
Ball	ZrO ₂
Disk	K417G alloy, NiAlTa coating
Temperature(°C)	25, 800
Heat rate(°C/min)	10
Load(N)	20
Rotation speed(rpm)	60
Time(s)	3600
Radius(mm)	15

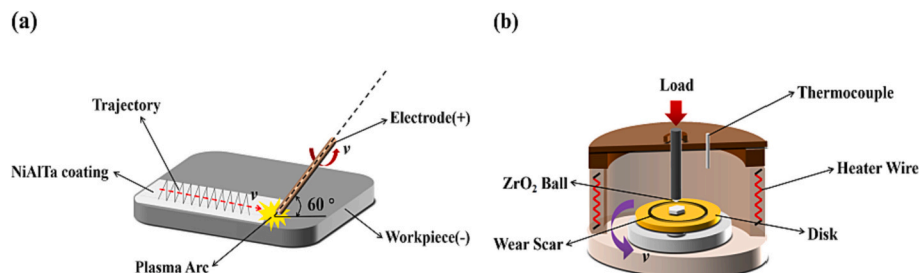


Fig. 1. Schematic diagram of the electro spark deposition principle (a) and the friction and wear principle (b).

wear track, mm.

$$V = \int_{\sqrt{\frac{4D^2 - d^2}{4}}}^d \pi(d^2 - y^2) dy \quad (2)$$

where V is the wear volume of the ZrO_2 ball, mm^3 ; d is the radius of the ZrO_2 ball, mm; and D is the diameter of the wear track, mm. The wear rate was calculated by substituting the obtained wear volumes into Eq. (3):

$$W_r = \frac{V}{PS} \quad (3)$$

where W_r is the wear rate, $mm^3 \cdot N^{-1} \cdot m^{-1}$; V is the wear volume, mm^3 ; P is the load, N; and S is the sliding distance, m.

3. Results

3.1. Microstructure and phase composition of electrodes and deposited coatings

Fig. 2 shows the X-ray diffraction (XRD) patterns of the electrode and the deposited coating. The XRD results show that the electrode is mainly composed of the β -NiAl phase and the laves phase NiTaAl. In addition to these two phases, a small amount of AlTa phase can also be found in the deposited coating. The excess Ta element, which was captured by the Al element, generated the AlTa phase [13]. The diffraction peak of the β -NiAl phase shows a shift to the left side compared with the standard diffraction peak due to the dissolution of other atoms with larger atomic radii, such as Ta, in the lattice of the β -NiAl phase.

Fig. 3 shows the microstructure of the electrode (a) and the deposited coating (b) and the corresponding energy dispersive spectroscopy (EDS) analysis results. Combined with EDS and XRD results (Fig. 2), the dark and light phases in Fig. 3a and b are the β -NiAl and NiTaAl phases, respectively. The microstructure of the electrode shows that the primary phase β -NiAl is surrounded by NiAl-NiTaAl eutectic (Fig. 3a) [11]. Unlike the microstructure of the electrode, the NiAlTa coating has a fine and uniform “cell-like” structure (Fig. 3b). The “cells” composed of the β -NiAl phase show a regular shape and a uniform size (approximately 550 nm). The continuous distribution of the laves phase NiTaAl forms the “cell wall” of the β -NiAl phase. The NiAl phase is encapsulated by the laves phase NiTaAl, which is similar to the plant “cell wall” structure. This structure can provide the coating with excellent high-temperature strength and mechanical properties. In addition, the NiAl-NiTaAl

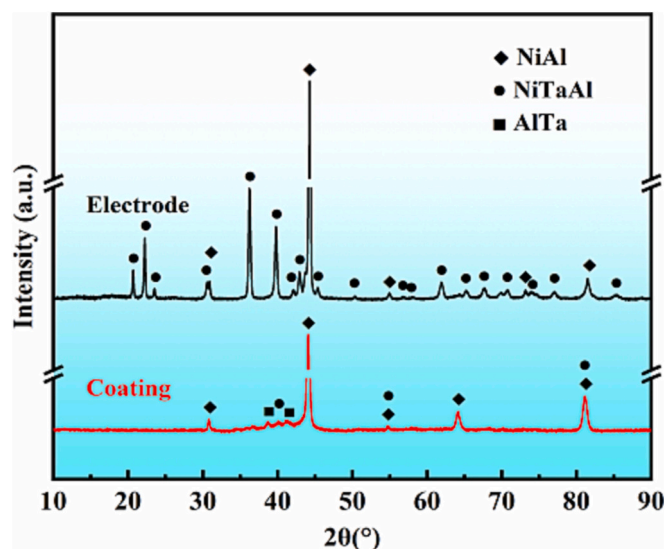


Fig. 2. XRD patterns of the electrode and deposited coating.

eutectic structure can be found in the coating.

3.2. Microhardness and bond strength of the coatings

Fig. 4a shows the microhardness distribution of the electrode and coating-substrate cross-section. Fig. 4a reveals that the average microhardness of the coating (797.18 $HV_{0.2}$) is approximately twice that of the substrate (391.63 $HV_{0.2}$), which is sufficient to expect for the coating to have better wear resistance and cutting performance than the substrate. Compared with those of the substrate and the coating, the microhardness distribution of the electrode is extremely heterogeneous (617.14 $HV_{0.2}$), which is directly related to the microstructure or phase distribution. The microhardness of the coating is significantly higher than that of the electrode in the case of the same phase composition, which is related to factors such as the ultra-fine microstructure and the redistribution of phases.

Fig. 4b shows the scratch morphology of NiAlTa coating and the corresponding friction force and acoustic emission signals. It can be found from Fig. 4b that the coating is mainly deformed by plasticity in the whole scratch experiment. When the load is 47.56 N, the coating starts to be damaged. Significant plastic deformation of the coating occurs. When the load is increased to 85.20 N, the bright white substrate is almost completely exposed, which indicates that the NiAlTa coating has completely failed. This load is better than the critical load required for general engineering applications (~ 30 N), which indicates that the NiAlTa coating has excellent adhesion strength to the K417G substrate.

3.3. Tribological behavior

Fig. 5a shows the real-time friction coefficients of the K417G substrate and the NiAlTa coating sliding with ZrO_2 balls. The figure indicates that the friction coefficients of the K417G substrate and the NiAlTa coating show a decreasing trend with the increasing temperature, and the change is more significant for the K417G substrate. At 25 °C, the friction coefficient of the K417G substrate is higher than that of the NiAlTa coating. However, the friction coefficient of the NiAlTa coating is significantly higher than that of the K417G substrate at 800 °C. Unlike the K417G substrate, the friction coefficient of the NiAlTa coating fluctuates greatly in the latter stage and eventually tends to stabilize at a certain value (0.45–0.50). This trend may be related to the destruction of the transfer film by hard particles.

The wear rates and average friction coefficients of the K417G substrate and the NiAlTa coating sliding with ZrO_2 balls as a function of temperature are shown in Fig. 5b. At 800 °C, the wear volume of the NiAlTa coating is extremely small to measure and therefore not shown in Fig. 5b. Fig. 5c shows the 2D profiles of the K417G substrate and the NiAlTa coating at different temperatures. Consistent with the variation of the average friction coefficient, the wear rates of the K417G substrate and the NiAlTa coating gradually decrease with the increasing temperature (Fig. 5b). The wear rate of the K417G substrate ($\sim 10^{-5} mm^3 \cdot N^{-1} \cdot m^{-1}$) is significantly higher than that of the NiAlTa coating ($\sim 10^{-6} mm^3 \cdot N^{-1} \cdot m^{-1}$, 25 °C). Notably, the wear profile of the NiAlTa coating differs from the typical “U” or “V” profile at 800 °C (Fig. 5c), and the wear volume at this point is extremely small to measure. In addition, the wear width of the K417G substrate gradually decreases (from 1310 μm to 730 μm) with the increase in temperature, but the wear depth gradually increases (from 24 μm to 32 μm). Unlike the K417G substrate, the variation trend of the wear width and depth with the temperature for the NiAlTa coating is opposite that of the K417G substrate (Fig. 5c). The wear depth of the NiAlTa coating at different temperatures is much smaller than that of the substrate. The above experimental results reveal that the NiAlTa coating has superior wear resistance over the K417G substrate.

Fig. 5d shows the wear rate of counterpart ZrO_2 balls as a function of temperature. ZrO_2 balls ground against the K417G substrate and NiAlTa coating are noted as K417G- ZrO_2 and NiAlTa- ZrO_2 , respectively.

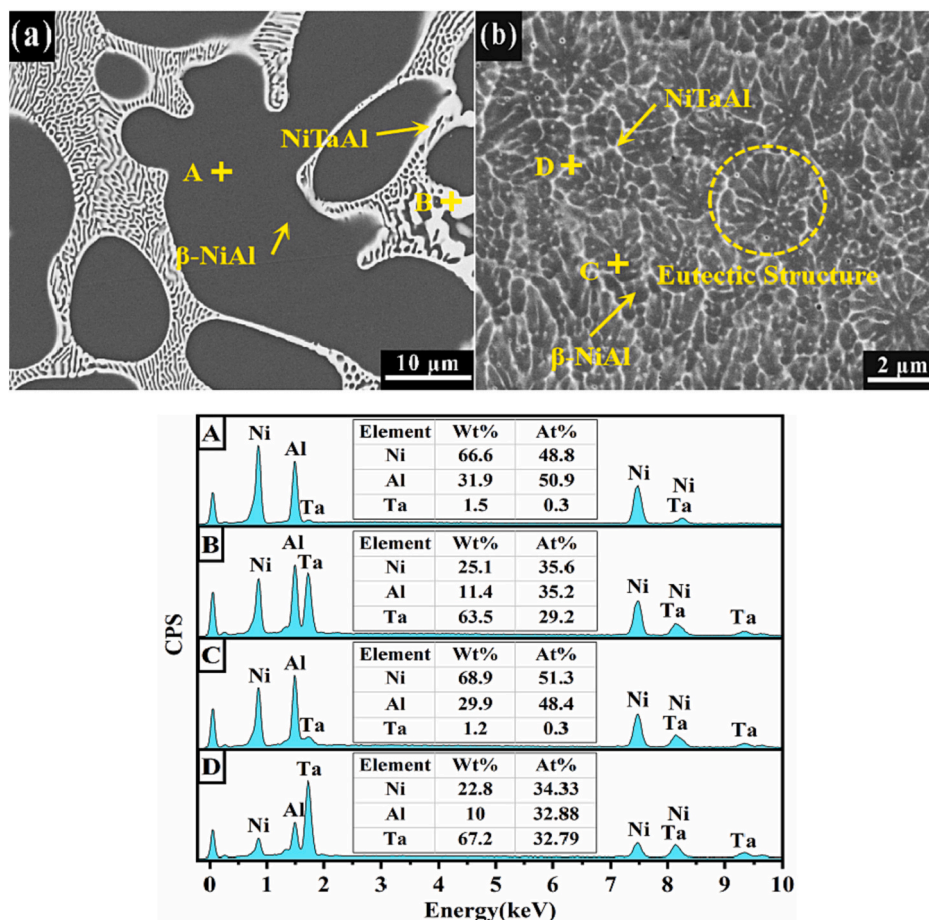


Fig. 3. Microstructure and corresponding EDS analysis results of the electrode (a) and the NiAlTa coating (b).

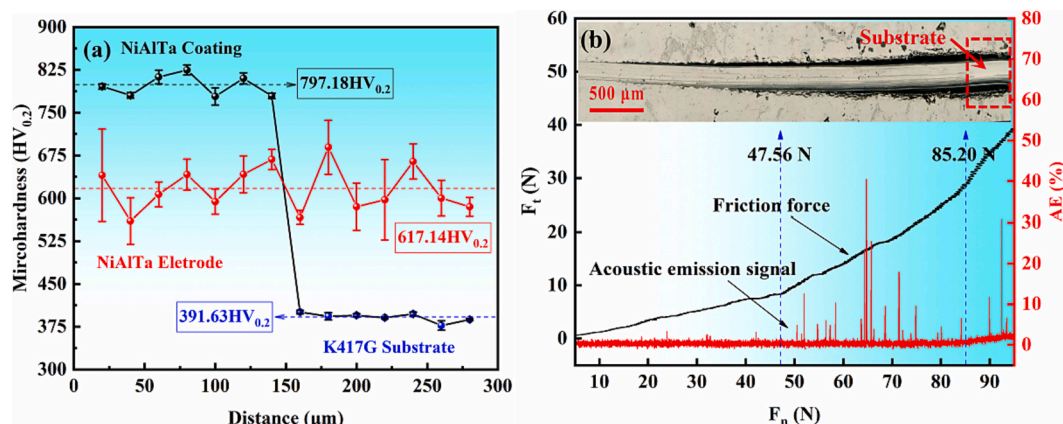


Fig. 4. Microhardness distribution of electrode and coating-substrate cross-section (a), the scratch morphology of NiAlTa coating and the corresponding friction force and acoustic emission signals (b).

Unpolished NiAlTa coating is used in practical applications, so the wear rate of ZrO₂ balls sliding with the unpolished NiAlTa coating is as provided in Fig. 5c and labeled as unpolished NiAlTa-ZrO₂. The figure shows that the wear rate of K417G-ZrO₂ decreases from $\sim 10^{-5}$ mm³·N⁻¹·m⁻¹ to $\sim 10^{-6}$ mm³·N⁻¹·m⁻¹ as the temperature increases. In contrast to the wear rate trend of K417G-ZrO₂, the wear rate of NiAlTa-ZrO₂ increases from $\sim 10^{-6}$ mm³·N⁻¹·m⁻¹ to $\sim 10^{-4}$ mm³·N⁻¹·m⁻¹ with the increase of temperature. The wear rate of unpolished NiAlTa-ZrO₂ is greater than that of polished NiAlTa-ZrO₂ at different temperatures. At 800 °C, the wear rate increases significantly to $\sim 10^{-3}$ mm³·N⁻¹·m⁻¹. In

addition, the wear rates of both polished and unpolished NiAlTa-ZrO₂ are lower than those of K417G-ZrO₂ at 25 °C. In principle, the protective coating for blade tips should be designed to have good wear resistance and cutting performance. In this experiment, the wear rate of ZrO₂ reflects the cutting performance of the coating. Therefore, the above experimental results indicate that the NiAlTa coating has good wear resistance at both 25 °C and 800 °C. At 25 °C, the cutting performance of the NiAlTa coating is slightly inferior to that of the K417G substrate. However, the cutting performance of the NiAlTa coating is significantly better than that of the K417G substrate at 800 °C. The cutting

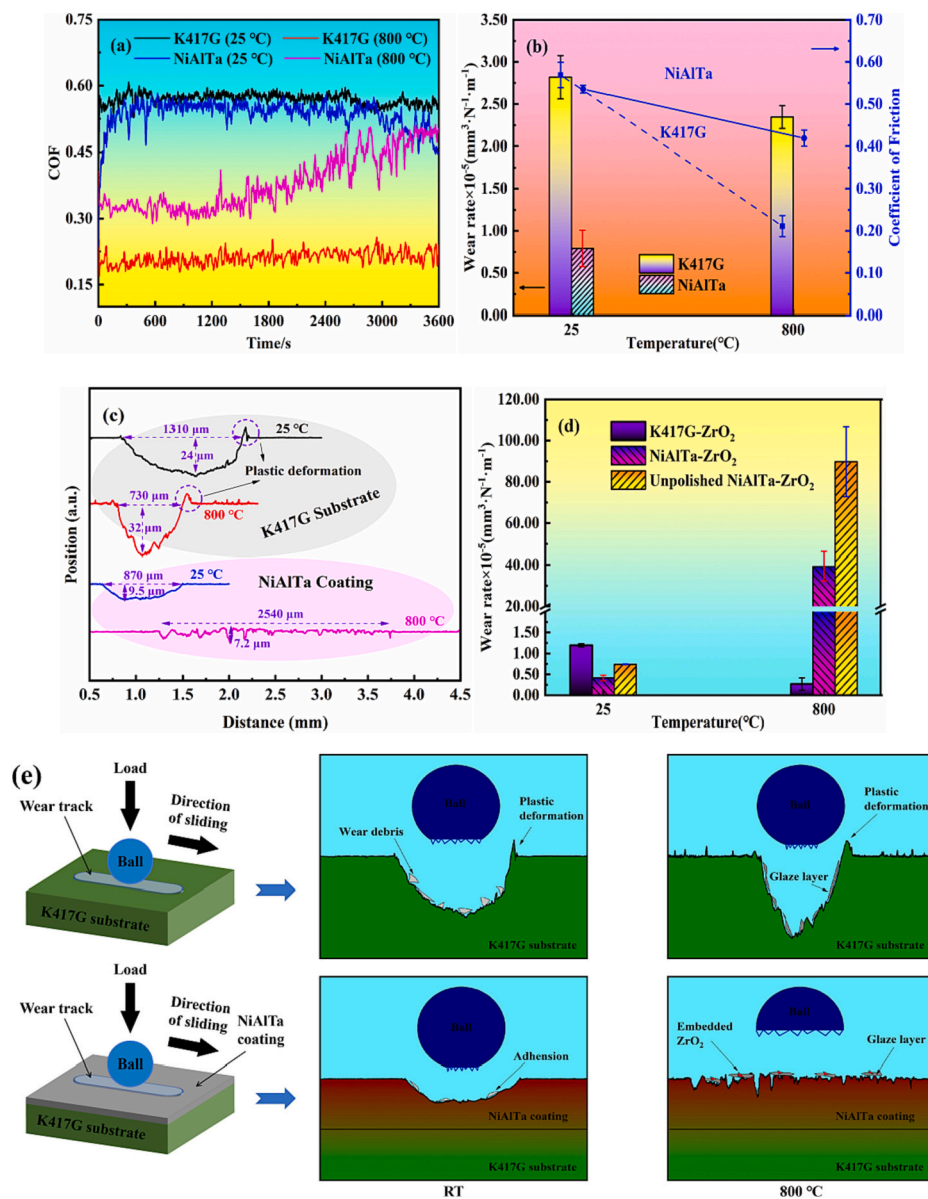


Fig. 5. Real-time friction coefficients of coating and substrate (a), average friction coefficients and wear rates of coating and substrate (b), 2D profiles of coating and substrate (c), and wear rates of ZrO₂ balls (d), the schematic map about the difference of the models for friction and wear between K417G substrate and NiAlTa coating (e).

performance of the unpolished coating is optimal.

Fig. 5e shows the schematic map about the difference of the models for friction and wear between K417G substrate and NiAlTa coating. From Fig. 5e, it can be seen that the tribological behavior of the substrate and coating at different temperatures is significantly different. This will be discussed in the next section.

To understand the tribological behavior of the K417G substrate and the polished or unpolished NiAlTa coating at 25 °C and 800 °C, the morphology of the worn surface was observed by scanning electron microscopy, and the results are shown in Fig. 6.

After the tribotest at 25 °C (Fig. 6a–b), the worn surface of the K417G substrate was rough, with obvious material bulge and accumulation (adhesions). The adhesions were produced by the repeated crushing and smearing of debris, and many micro grooves were distributed on the surface. Under the action of cyclic stress, spalling occurred on the surface of certain adhesions due to repeated adhesions and shear deformations. The worn surface of the NiAlTa coating was smooth and flat, except for few adhesions and micro-spalling pits, which are mainly

dominated by micro grooves (Fig. 6b enlarged view).

After the tribotest at 800 °C (Fig. 6c–d), the worn surface of the K417G substrate was covered with a continuous flat and smooth black film, that is, the “glaze” layer. The surface of the “glaze” layer had many grooves and spalling pits. The local magnification reveals extremely fine and spherical-shaped debris inside the hole. This feature is typical of the oxidation wear of coatings at high temperatures [7,14]. These extremely fine debris fragments have been reported to be a sign of “glaze” layer formation [7,14,15]. The support of the substrate to the “glaze” layer decreases significantly with the increase in temperature, while the “glaze” layer begins to flake under the cyclic stress of the ceramic ball and the plowing action of hard particles.

Numerous milky white adhesions can be found on the worn surface of the NiAlTa coating. Milky white adhesions were distributed in a discontinuous black “glaze” layer. EDS analysis shows that the adhesion was mainly composed of Zr, Ni, Al, O, and other elements. The fine metal oxide and ZrO₂ debris were mixed, compacted, and sintered under the combined effect of high temperature and cyclic stress, forming a special

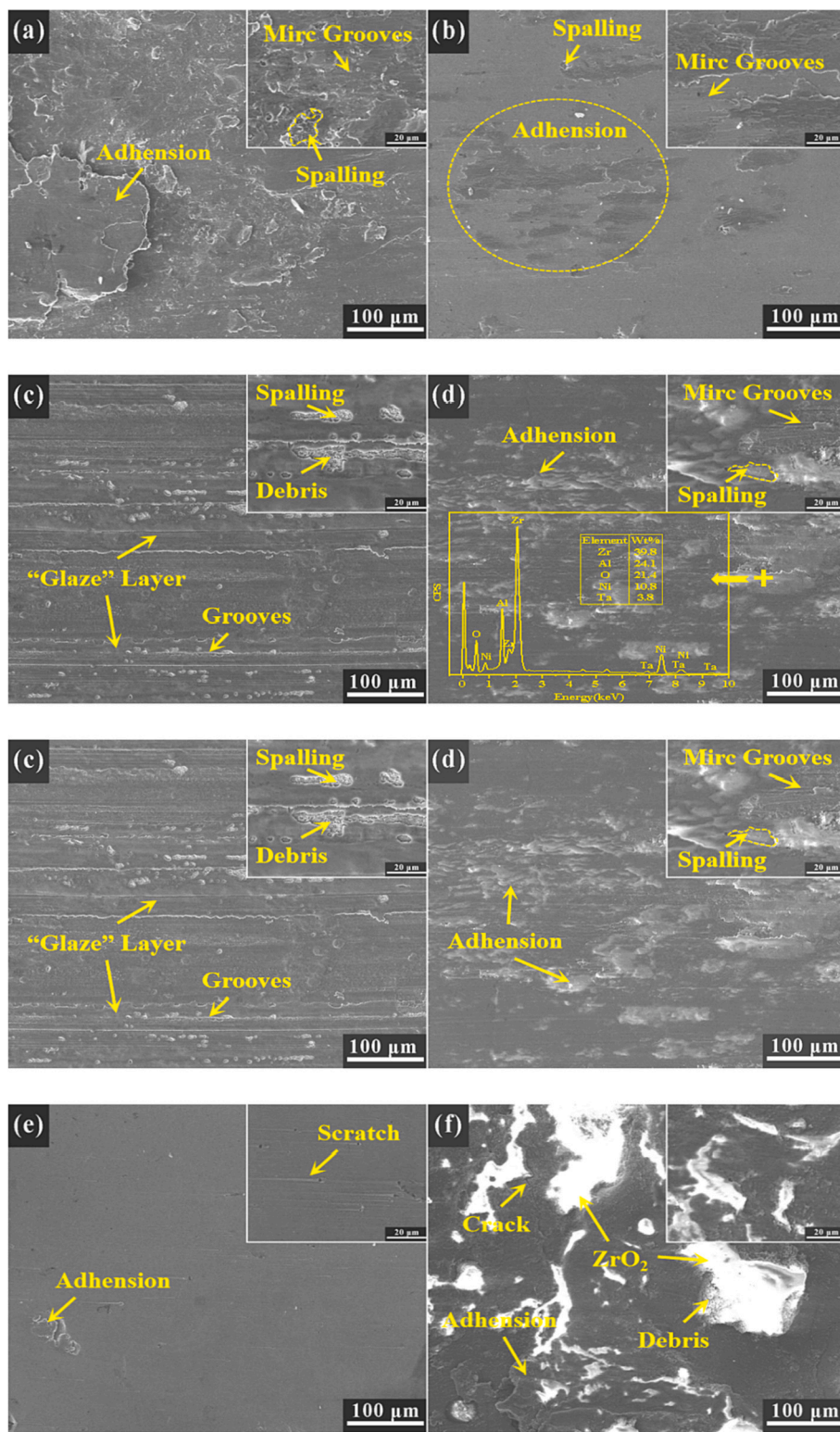


Fig. 6. Worn surfaces of K417G substrate and NiAlTa coating at 25 °C and 800 °C. (a) K417G at 25 °C; (b) NiAlTa at 25 °C; (c) K417G at 800 °C; (d) NiAlTa at 800 °C; (e) Unpolished NiAlTa at 25 °C; (f) Unpolished NiAlTa at 800 °C. The inset of the figure is an enlarged view of the local area.

“glaze” layer + ZrO₂ structure. The local magnification reveals that the area not covered by the “glaze” layer was full of micro grooves from the three-body abrasive wear caused by the hard oxide particles. In addition, the milky white adhesions embedded in the “glaze” layer were flaking off.

Fig. 6e–f shows the worn surface of the unpolished NiAlTa coating at

25 °C and 800 °C. At 25 °C, only a few scratches could be observed on the worn surface of the NiAlTa coating. Compared with the polished coating, the number of adhesions on the worn surface of the unpolished coating was significantly reduced. At 800 °C, numerous milky white ZrO₂ debris were embedded on the coating surface. The size and number of the embedded ZrO₂ in the unpolished coating are larger than those in

the polished coating (Fig. 6d). A thermal mismatch occurred between the metal phase and the oxide ceramic interface with the increase in temperature, and the interfacial bond between them weakened. Some cracks along the boundary between the metal and the ceramic were found at the edge of ZrO_2 .

To better understand the tribological behavior of the K417G substrate and the NiAlTa coating, the worn surfaces of the ZrO_2 balls sliding with the K417G substrate and the NiAlTa coating at 25 °C and 800 °C are shown in Fig. 7. The figure shows that severe material transfer from the K417G substrate to the surface of ZrO_2 ceramic balls occurred at both room and high temperatures, forming a continuous layered transfer film on the surface of the ceramic balls (Fig. 7a and c). The transfer film showed discontinuous features and was covered with many micro grooves. At 25 °C, the NiAlTa coating transferred to the surface of the ZrO_2 ceramic balls. Many debris could be observed on the worn surface. When the temperature increased to 800 °C, the material transfer phenomenon was significantly suppressed. At this time, numerous cutting marks and debris could be observed on the surface of the ZrO_2 ceramic ball. The worn surface of the ZrO_2 ball sliding with the unpolished coating is very similar to that of the polished coating. At 800 °C, the surface of the ZrO_2 ceramic balls was covered with many grooves. The

debris in Fig. 7d is nearly completely removed, indicating that the unpolished NiAlTa coating results in a good cutting of ZrO_2 ceramic balls.

4. Discussion

4.1. Effects of microstructure and phase composition on mechanical properties and tribological behavior of coatings

The ESD technique has ultra-high temperature gradient and cooling rate. These inherent properties can inhibit the coarsening of the coating microstructure and solute separation, allowing the good homogenization of the coating [12]. The unidirectional rapid solidification near one dimension allows the primary phase β -NiAl to assume a nanostructure (Fig. 3b) while allowing the dissolved elements to obtain a supersaturated solid solution (i.e., β -NiAl(Ta)) before they are separated. This finding is confirmed by the shift of the diffraction peak of the β -NiAl phase to the left as shown in Fig. 2. Subsequently, the excess Ta reacts with Ni and Al to form continuous “mesh-like” laves phase NiTaAl at the grain boundary of nanophase β -NiAl or the eutectic cell boundary (Fig. 3b).

The phase composition and microstructure of the coating affect the

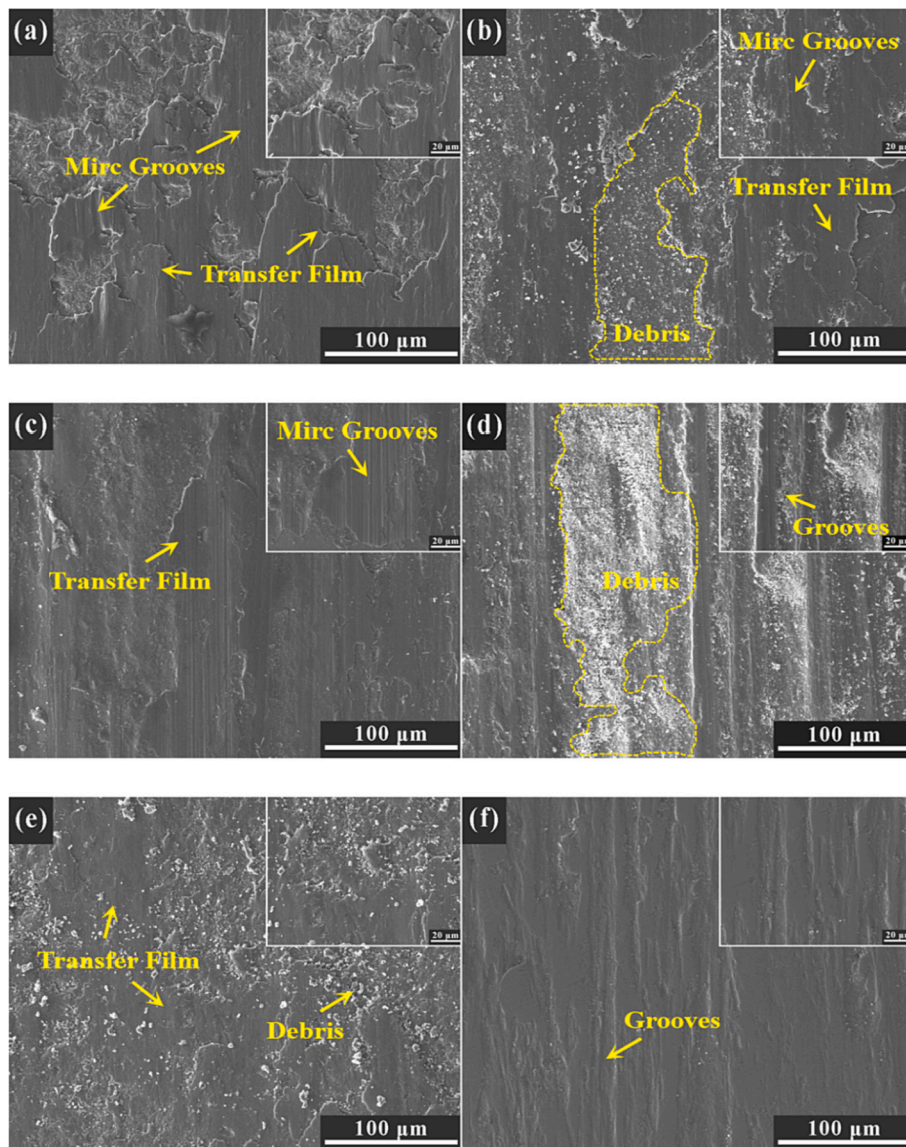


Fig. 7. The worn surface of ZrO_2 balls sliding with the K417G substrate and NiAlTa coating at 25 °C and 800 °C. (a) K417G at 25 °C; (b) NiAlTa at 25 °C; (c) K417G at 800 °C; (d) NiAlTa at 800 °C; (e) Unpolished NiAlTa at 25 °C; (f) Unpolished NiAlTa at 800 °C. The inset of the figure is an enlarged view of the local area.

mechanical properties of the coating and thus affect the tribological behavior of the coating. The β -NiAl phase is characterized by the coexistence of metallic and covalent bonds and is a Hume–Rothery electronic compound between metal and ceramic [16]. The β -NiAl phase itself has a high hardness. The laves phase NiTaAl is a topologically closed-packed phase with an extremely small interatomic spacing and a high space occupancy [2,11,17]. Thus, the laves phase usually also has a high hardness. The combination of the β -NiAl phase and laves phase NiTaAl results in an ultra-hard coating, which also leads to a smaller wear rate compared to the substrate (Figs. 4, 5b and c). Meanwhile, the β -NiAl and NiTaAl phases are characterized by strong interatomic bonding with mainly covalent bonds, endowing them with excellent anti-adhesive wear properties and low friction coefficients (Figs. 5a, 6b, and d). It is well known that the room temperature brittleness of β -NiAl phase is large, which is usually considered unfavorable in friction and wear. However, in this study, the wear process of the NiAlTa coating was mainly plastic deformation under the condition of compressive stress, and nearly no evidence of material loss through brittle fracture could be found (Fig. 6b and d–f). This result is unexpected and indicates that the NiAlTa coating is suitable for compressive stress conditions. In addition, the skeleton structure formed by the eutectic lamellae and fine grains in the fast-setting alloy can effectively inhibit the generation and extension of cracks [18,19].

In high-temperature deformation, the plasticity of NiAl alloys increases abruptly (>20 %) once the ductile–brittle transition temperature (350 °C–400 °C) is exceeded or approached [19]. At 800 °C, the content and distribution of laves phase NiTaAl are the main factors affecting the high-temperature strength and tribological behavior of the coating at high temperatures. Fig. 3b shows that a large amount of laves phase NiTaAl encapsulates the NiAl phase, which is similar to a plant “cell wall” structure that allows the NiTaAl phase to function as a stress transfer and load support during the high-temperature wear process, thus delaying the increase of the real contact area between the ceramic ball and the coating. This finding is confirmed by the minimal wear rate at high temperatures (Fig. 5b). In addition, at 800 °C, the combination of NiAl phase with good high-temperature toughness and NiTaAl phase with high-temperature strength can not only effectively coordinate the local deformation but also provide good load support capability, which significantly reduces the wear rate of the coating (Fig. 5b and Fig. 5c).

4.2. Analysis of wear mechanisms of the substrate and the coating at 25 °C and 800 °C

At 25 °C, the ZrO₂ ceramic balls are pressed into the substrate under load, causing a significant plastic deformation of the substrate surface. Subsequently, under the action of friction force, the hard phase ZrO₂ ceramic ball plows the soft phase substrate, and serious material bulge and accumulation occur (Fig. 6a). Meanwhile, serious material transfer also occurs between the friction pairs (Figs. 7a–d). The characteristics of the torn adhesive joints on the worn surface of the K417G substrate indicate that a significant adhesion–shear phenomenon occurs during the sliding process (Fig. 6a), which results in relatively high friction coefficient and wear rate (Fig. 5a and b). This phenomenon is mainly attributed to the adhesive wear caused by the FCC phase (γ -Ni phase) with many slip systems and a high crystal structure symmetry in the K417G substrate [20,21]. However, the NiAlTa coating with high hardness resists most of the plastic deformation and reduces the contact area between the ceramic ball and the alloy, thus reducing the wear rate of the coating (Fig. 5b). Therefore, the wear process of NiAlTa coatings is still dominated by a small amount of plastic deformation.

The microhardness measurement of the worn surface shows (Table 4) that the K417G substrate and the NiAlTa coating undergo significant work hardening during the wear process, and the hardness of the adhesions on the worn surface is much greater than that on the substrate. These high hardness adhesions cause some damage to the ceramic balls during the wear process (Figs. 5d, 7a, and b). The work

Table 4
Microhardness data from worn samples.

Materials	Vickers hardness(25 °C)
K417G substrate	
Bulk material (unworn)	391.63 HV _{0.2}
Wear scar	586.16 HV _{0.2}
Wear debris	732.39 HV _{0.2}
NiAlTa coating	
Bulk material (unworn)	797.18 HV _{0.2}
Wear scar	894.08 HV _{0.2}
Wear debris	1009.78 HV _{0.2}

hardening results indicate the downward trend of the real-time friction coefficient curves of the substrate and the coating show in the latter stage (Fig. 5a). In addition, the presence of work hardening reduces the wear rate of both the coating and the substrate.

The friction coefficient and wear rate of the K417G substrate and the NiAlTa coating change significantly with the increase in temperature (Fig. 5a). This change is related to the changes in the microstructure and mechanical properties of the coating and the substrate at high temperatures but more directly related to oxidation. On the one hand, oxidation causes the loss of strengthening elements in the coating and the substrate, leading to a decrease in surface bearing capacity. On the other hand, the oxidation products and their contents on the worn surface will inevitably have an important influence on the wear mechanism of the coating. Therefore, the phase composition and evolution of the worn and unworn surfaces of the K417G substrate and the NiAlTa coating must be analyzed at different temperatures.

Fig. 8 shows the X-ray patterns and Raman spectra of the worn and unworn surfaces of the K417G substrate and the NiAlTa coating at 800 °C. At 800 °C, the K417G substrate generates a thin mixed oxide layer by static oxidation, mainly containing MoO₃ [22], Cr₂O₃ [23], Al₂O₃ [24], and NiCr₂O₄ (Fig. 8a and d). During the wear process, NiO [25] and NiAl₂O₄ [26] are generated on the worn surface under the combined effect of cyclic stress and high temperature (Fig. 8d). The highest intensity of the scattering peak of NiAl₂O₄ within the worn surface indicates that the worn surface is mainly composed of the NiAl₂O₄ spinel. The temperature of the worn surface of the K417G substrate can be roughly estimated from the model for estimating the frictional heat [27]:

$$T_c = T_b + \Delta T_f \quad (4)$$

$$\Delta T_f = \frac{\mu v \sqrt{\pi F_n \sigma_{0.2}}}{8\lambda} \quad (5)$$

where T_c is the friction surface temperature, T_b is the experimental temperature (800 °C), ΔT_f is the maximum instantaneous flash temperature, μ is the friction coefficient (0.211), v is the sliding speed (0.094 m/s), F_n is the normal load (15 N), $\sigma_{0.2}$ is the yield strength (~825 MPa), and λ is the thermal conductivity (~13.2 W/(m·°C)). The worn surface temperature of the K417G substrate is approximately 837.03 °C. This temperature is near the formation temperature of the NiAl₂O₄ spinel (~850 °C) [28]. Therefore, the frictional chemical reactions initiated by the instantaneous heat and stress generated during the friction process eventually lead to the formation of a large amount of spinel, that is, NiO + Al₂O₃ = NiAl₂O₄.

The phase evolutions of polished or unpolished NiAlTa coatings at 800 °C are nearly the same (Fig. 8b–c and e–f), and only the intensity of the diffraction peak changes. Taking the polished coatings as an example (Fig. 8b and e), the oxidation products of the coatings are mainly dominated by NiTa₂O₆ [29], AlTaO₄, and Al₂O₃. Under the dual action of friction heat and ambient temperature, the internal oxidation of the worn surface is serious, and the new NiAl₂O₄ spinel appears. In addition, many scattering peaks of ZrO₂ are detected on the worn surface [30].

unpolished coating is good. Obviously, the difference in cutting performance is related to the oxidation products, the structure of the friction layer, and the microstructure or strength change of the coating at high temperatures.

At 25 °C, effectively cutting the hard ZrO₂ balls is difficult for the soft phase coating, and shearing occurs mainly in the coating. The exfoliated metal debris undergoes significant work hardening during the reciprocating sliding process (the results in Table 4 show that the hardness of the adhesions (1009.78 HV_{0.2}) is near that of the ceramic ball (1215 HV_{0.2})), which causes the hardened adhesions to partially plow the ceramic ball. However, the adhesions with high hardness are few and thin (Fig. 6b), so the cutting effect of the NiAlTa coating on the ZrO₂ ball at room temperature is insignificant.

At 800 °C, Figs. 8e–f shows a large amount of low ionic potential oxides (such as Al₂O₃, $\phi = 6$) inside the worn surface when the cutting performance of the NiAlTa coating reaches a high level. The three-body abrasive wear caused by these oxides with low ionic potential is considered to be the cause of the cutting performance of the NiAlTa coating at high temperatures. Subsequently, the two-body abrasive wear induced by the ZrO₂ debris embedded in the “glaze” layer aggravates the plowing. In addition, compared with the deposited coating (Fig. 2), the diffraction peaks of the β -NiAl phase shift to the left side by 3° (Figs. 8b–c). The crystal plane spacing decreases, indicating the precipitation of solute Ta elements in the β -NiAl(Ta) solid solution at high temperatures. Meanwhile, the relative peak intensities of the diffraction peaks of laves phase NiTaAl are significantly high (Figs. 8b–c), indicating that the precipitated Ta elements react with Ni and Al elements to produce more high-temperature resistant phase NiTaAl. In addition, the Al₄Ni₃ phase is formed in the NiAlTa coating. The strength loss of the ZrO₂ ceramic balls at high temperature is serious, while the increase of the NiTaAl content and the generation of the Al₄Ni₃ phase suppress the high-temperature strength loss of the coating to some extent. At this time, the hard phase NiAlTa coating plows the soft phase ZrO₂, while the high temperature strength provides good mechanical support for the cutting of the low ionic potential oxide or ZrO₂ debris. Therefore, the cutting effect of the NiAlTa coating on ZrO₂ balls at high temperatures is remarkable. This finding is confirmed by the smooth worn surface (covered with grooves) of the ZrO₂ ceramic balls (Fig. 7d and f).

The excellent cutting performance of the unpolished coating can be attributed to the following reasons: the mechanical shearing of the ZrO₂ ceramic balls by the microconvex body with high stress, and the highly intense oxidation of the rough coating, which generates more oxidation products with low ionic potential and intensifies the occurrence of three-body abrasive wear. Subsequently, the occurrence of intensified ZrO₂ debris-induced two-body abrasive wear is triggered.

5. Conclusions

In this paper, the high-temperature tribological behavior of the “NiAlTa coating + ESD” system was evaluated. The experimental results showed that this system was a promising candidate for a blade tip protective coating system under high temperature condition. Next, in addition to the optimization of the preparation process parameters, the high speed rubbing behavior of the coating (> 300 m/s) will be investigated and evaluated using a test machine simulating the actual working conditions of the aeroengine.

- (1) The NiAlTa coating mainly consists of the nano scale β phase NiAl and the continuously distributed mesh structure laves phase NiTaAl. Laves phase NiTaAl surrounded by NiAl phase endows the coating with excellent mechanical properties, wear resistance, and cutting performance.
- (2) Compared with the K417G substrate, NiAlTa coating has higher microhardness (~ 797.18 HV_{0.2}) and lower wear rate ($\sim 10^{-6}$ mm³·N⁻¹·m⁻¹). Scratch test shows that NiAlTa coating has excellent bonding strength with substrate.

- (3) The competition between the wear-reducing lubricating effect of the “glaze” layer and the plowing effect of oxides and ZrO₂ debris affects the friction coefficient and the wear rate of the coating. The wear process of NiAlTa coatings is dominated by plastic deformation.
- (4) The cutting performance is related to the oxidation products, the structure of the friction layer, and the microstructure or strength change of the coating. The two- or three-body abrasive wear caused by oxides and ZrO₂ debris is the main factor of the cutting performance.

CRedit authorship contribution statement

Shuai Yang: Data curation, Formal analysis, Methodology, Roles/ Writing-original draft.

Siyang Gao: Investigation, Supervision, Writing-review & editing.

Weihai Xue: Investigation, Writing-review & editing.

Bi Wu: Conceptualization, Methodology.

Deli Duan: Funding acquisition, Project administration, Resources, Supervision.

Declaration of competing interest

The authors declare that they have no known competing financial interests or personal relationships that could have appeared to influence the work reported in this paper.

Data availability

The raw/processed data required to reproduce these findings cannot be shared at this time as the data also forms part of an ongoing study.

Acknowledgements

The authors wish to thank Liaoning Key Laboratory of Aero-engine Material Tribology for both financial and facility support.

References

- [1] B. Yu, H.W. Ke, E.Y. Shen, T.H. Zhang, A review of blade tip clearance-measuring technologies for gas turbine engines, *Meas. Control-UK* 53 (2020) 339–357.
- [2] J.R. Davenport, L. Mendez-Garcia, S. Purkayastha, M.E. Hancock, R.J. Stearn, W. J. Clegg, Material needs for turbine sealing at high temperature, *Mater. Sci. Technol.* 30 (2014) 1877–1883.
- [3] S. Yang, S.Y. Gao, W.H. Xue, B. Wu, H. Cheng, D.L. Duan, Epitaxial growth and oxidation behavior of the NiCoCrAlYTa/Y2O3 coating on a nickel-based single-crystal superalloy blade tips, produced by electro spark deposition, *J. Alloys Compd.* 931 (2023), 167600.
- [4] X.M. Sun, L.Z. Du, H. Lan, H.F. Zhang, R.Y. Liu, Z.G. Wang, S.G. Fang, C.B. Huang, Z.A. Liu, W.G. Zhang, Study on thermal shock behavior of YSZ abradable sealing coating prepared by mixed solution precursor plasma spraying, *Surf. Coat. Technol.* 397 (2020), 126045.
- [5] Tribomet Abrasive Coatings. <http://www.praxairsurface.com/-/media/corporate/praxairsurface/us/documents/brochures/tribomet-abrasive-coatings.pdf>, 2010 (accessed December 2019).
- [6] Y.D. Liu, J. Sun, Z.L. Pei, W. Li, J.H. Liu, J. Gong, C. Sun, Oxidation and hot corrosion behavior of NiCrAlYSi+NiAl/cBN abrasive coating, *Corros. Sci.* 167 (2020), 108486.
- [7] G. Bolelli, C. Vorkötter, L. Lusvardi, S. Morelli, V. Testa, R. Vassen, Performance of wear resistant MCrAlY coatings with oxide dispersion strengthening, *Wear* 444 (2020), 203116.
- [8] Y.D. Liu, J.P. Zhang, Z.L. Pei, J.H. Liu, W.H. Li, J. Gong, C. Sun, Investigation on high-speed rubbing behavior between abrasive coatings and Al/hBN abradable seal coatings, *Wear* 456 (2020), 203389.
- [9] J.A. Haynes, B.A. Pint, W.D. Porter, I.G. Wright, Comparison of thermal expansion and oxidation behavior of various high-temperature coating materials and superalloys, *Mater. High Temp.* 21 (2004) 87–94.
- [10] H. Hu, S.R. Li, Y.S. Ren, W.G. Liu, H. Zhao, Site preference and brittle-ductile transition mechanism of B2-NiAl with ternary elements additions from first-principles calculations, *Physica B* 576 (2020), 411703.
- [11] M. McGregor, Ni-Al-Ta Alloys for High Temperature Abrasive Coatings, University of Cambridge, 2019.
- [12] Y. Xie, M. Wang, Epitaxial MCrAlY coating on a Ni-base superalloy produced by electrospark deposition, *Surf. Coat. Technol.* 201 (2006) 3564–3570.

- [13] M. Müller, A. Stellmacher, M. Riede, E. López, F. Brueckner, C. Leyens, Multimaterial additive manufacturing of graded laves phase reinforced NiAlTa structures by means of laser metal deposition, *Adv. Eng. Mater.* 24 (2022), 2100993.
- [14] K. Feng, T. Shao, The evolution mechanism of tribo-oxide layer during high temperature dry sliding wear for nickel-based superalloy, *Wear* 476 (2021), 203747.
- [15] Y. Wang, X. Zhao, E. Hao, Z. Bu, Y. An, H. Zhou, J. Chen, High temperature induced “glaze” layer formed in HVOF-sprayed NiCrWMoCuCDBFe coating and its wear reduction mechanism, *Friction* 10 (2022) 1424–1438.
- [16] I.M. Robertson, C.M. Wayman, Tweed microstructures I. Characterization in β -NiAl, *Philos. Mag. A* 48 (1983) 421–442.
- [17] V. Raghavan, Al-Ni-Ta (aluminum-nickel-tantalum), *J. Phase Equilib. Diff.* 27 (2006) 405.
- [18] L.Y. Sheng, W. Zhang, C. Lai, J.T. Guo, T.P. Xi, H.Q. Ye, Microstructure and mechanical properties of laves phase strengthening NiAl base composite fabricated by rapid solidification, *Acta Metall. Sin.-Engl.* 49 (2013) 1318–1324.
- [19] J.T. Guo, *Ordered Intermetallic Compound NiAl Alloy*, Science Press, Beijing, 2003.
- [20] Y. Kao, T. Chen, S. Chen, J. Yeh, Microstructure and mechanical property of as-cast, homogenized, and deformed Al_xCoCrFeNi (0 < x < 2) high-entropy alloys, *J. Alloy Compd.* 488 (2009) 57–64.
- [21] D.B. Miracle, O.N. Senkov, A critical review of high entropy alloys and related concepts, *Acta Mater.* 122 (2017) 448–511.
- [22] M.Q. Wen, X.X. Chen, Z.B. Zheng, S.Z. Deng, Z.B. Li, W.L. Wang, H.J. Chen, In-plane anisotropic Raman spectroscopy of van der Waals α -MoO₃, *J. Phys. Chem. C* 125 (2020) 765–773.
- [23] H. Liu, Y. Feng, P. Li, X. Shi, H. Zhu, J. Shu, Q. Huang, F. Ge, F. Huang, Enhanced plasticity of the oxide scales by in-situ formed Cr₂O₃/Cr heterostructures for Cr-based coatings on Zr alloy in 1200 °C steam, *Corros. Sci.* 184 (2021), 109361.
- [24] C.T. Wang, Y.W. Ye, X.Y. Guan, J.M. Hu, Y.X. Wang, J.L. Li, An analysis of tribological performance on Cr/GLC film coupling with Si₃N₄, SiC, WC, Al₂O₃ and ZrO₂ in seawater, *Tribol. Int.* 96 (2016) 77–86.
- [25] A.Y. Faid, A.O. Barnett, F. Seland, S. Sunde, Ni/NiO nanosheets for alkaline hydrogen evolution reaction: in situ electrochemical-raman study, *Electrochim. Acta* 361 (2020), 137040.
- [26] S.S. Zhang, M. Ying, J. Yu, W.C. Zhan, L. Wang, Y. Guo, Y.L. Guo, Ni₃Al₂O₄- δ mesoporous catalysts for dry reforming of methane: the special role of NiAl₂O₄ spinel phase and its reaction mechanism, *Appl. Catal. B* 291 (2021), 120074.
- [27] F.P. Bowden, F.P. Bowden, D. Tabor, *The Friction and Lubrication of Solids*, Oxford University Press, New York, 2001.
- [28] N. Birks, G.H. Meier, F.S. Pettit, *Introduction to the High Temperature Oxidation of Metals*, Cambridge University Press, Cambridge, 2006.
- [29] S. Karmakar, B. Mukherjee, A.B. Garg, D.S. Gavali, R. Thapa, S. Banerjee, G. D. Mukherjee, A. Haque, D. Behera, Structural metamorphosis and band dislocation of trirutile NiTa₂O₆ under compression, *J. Phys. Chem. C* 126 (2022) 4106–4117.
- [30] J. Wang, L. Bai, F. Ma, S. Wan, G. Yi, J. Sun, X. Tian, Z. Yang, Evaluation of microstructure evolution of thermal barrier YSZ coating after thermal exposure, *Ceram. Int.* 48 (2022) 6681–6690.
- [31] A. Zhang, J. Han, B. Su, J. Meng, A novel CoCrFeNi high entropy alloy matrix self-lubricating composite, *J. Alloys Compd.* 725 (2017) 700–710.
- [32] A. Erdemir, A crystal-chemical approach to lubrication by solid oxides, *Tribol. Lett.* 8 (2000) 97–102.
- [33] A. Erdemir, A crystal chemical approach to the formulation of self-lubricating nanocomposite coatings, *Surf. Coat. Technol.* 200 (2005) 1792–1796.
- [34] Y. Yanliang, L. Shaolei, Z. Rui, W. Changyi, Z. Shengfeng, Influence of Al₂O₃ particles on the tribological properties of CoCrAlYTa coating produced by laser-induction hybrid cladding, *Ceram. Int.* 47 (2021) 19434–19442.
- [35] F. Ghadami, A. Zakeri, A.S.R. Aghdam, R. Tahmasebi, Structural characteristics and high-temperature oxidation behavior of HVOF sprayed nano-CeO₂ reinforced NiCoCrAlY nanocomposite coatings, *Surf. Coat. Technol.* 373 (2019) 7–16.